Supplement of Geosci. Model Dev., 19, 6001–6026, 2026
https://doi.org/10.5194/gmd-19-6001-2026-supplement

Geoscientific Model Development
Open Access
EGU

Supplement of

Evaluating the radiative fidelity of WRF-driven PALM (v25.04) in high-resolution using RTM: impact of diverse urban morphology and vegetation on short-wave radiation

Jelena Radović et al.

Correspondence to: Jelena Radović (jelena.radovic@matfyz.cuni.cz)

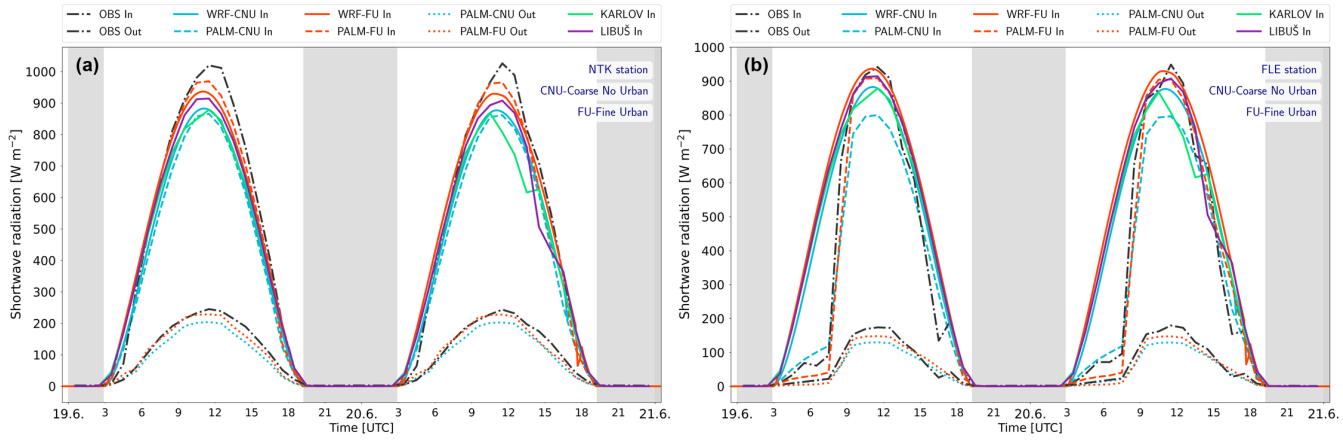

Figure S1. The comparison of observed hourly averages of incoming (In) and outgoing (Out) short-wave radiation for the e1 episode at the stations NTK (a) and FLE (b), with PALM model outputs for both WRF configurations. Additional lines represent the raw WRF outputs, Coarse No Urban (WRF-CNU), and Fine Urban (WRF-FU), and measurements from professional meteorological stations in Karlov and Libuš.

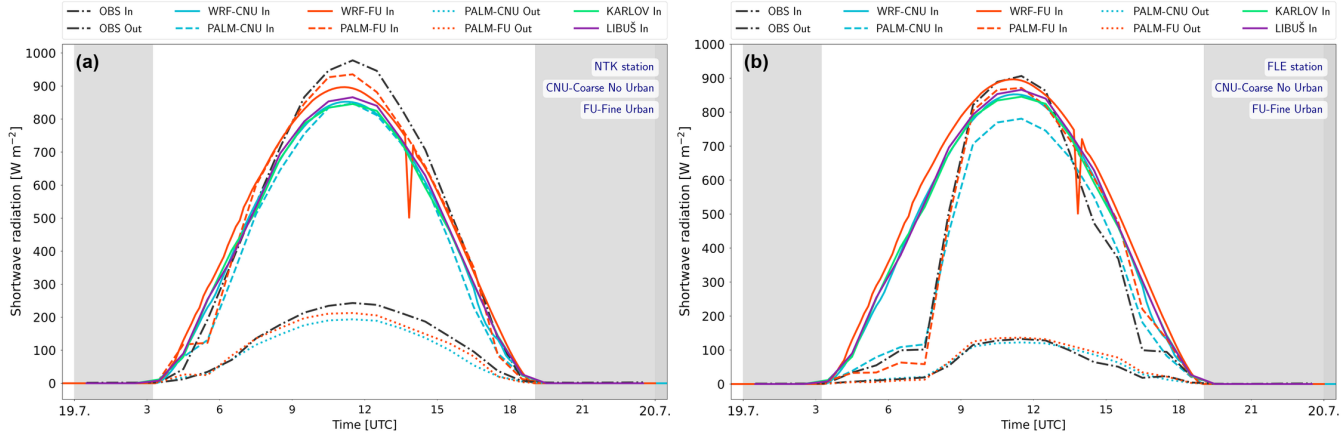

Figure S2. The comparison of observed hourly averages of incoming (In) and outgoing (Out) short-wave radiation for the e2 episode at the stations NTK (a) and FLE (b), with PALM model outputs for both WRF configurations. Additional lines represent the raw WRF outputs, Coarse No Urban (WRF-CNU), and Fine Urban (WRF-FU), and measurements from professional meteorological stations in Karlov and Libuš.

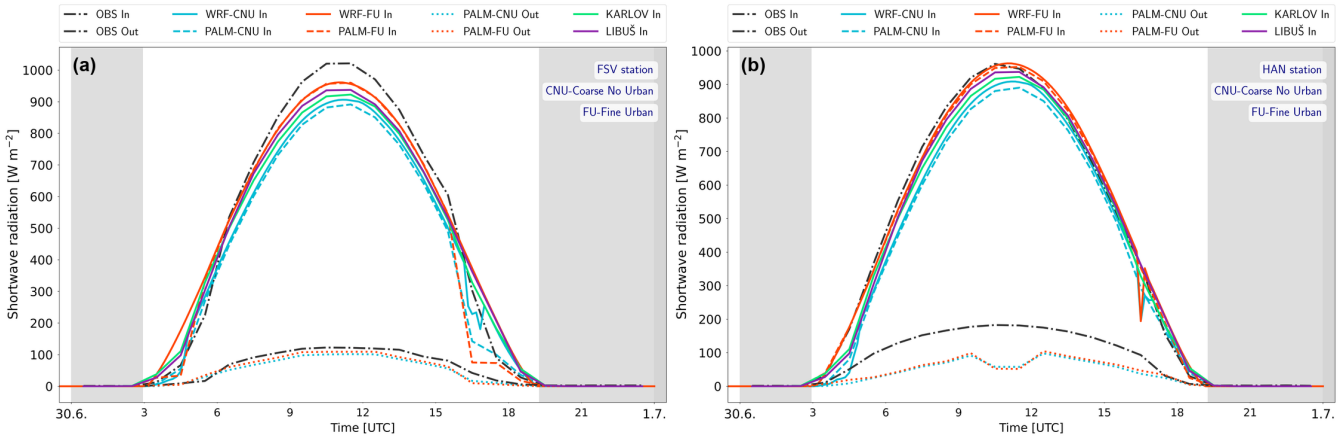

Figure S3. The comparison of observed hourly averages of incoming (In) and outgoing (Out) short-wave radiation for the e4 episode at the stations FSV (a) and HAN (b), with PALM model outputs for both WRF configurations. Additional lines represent the raw WRF outputs, Coarse No Urban (WRF-CNU), and Fine Urban (WRF-FU), and measurements from professional meteorological stations in Karlov and Libuš.

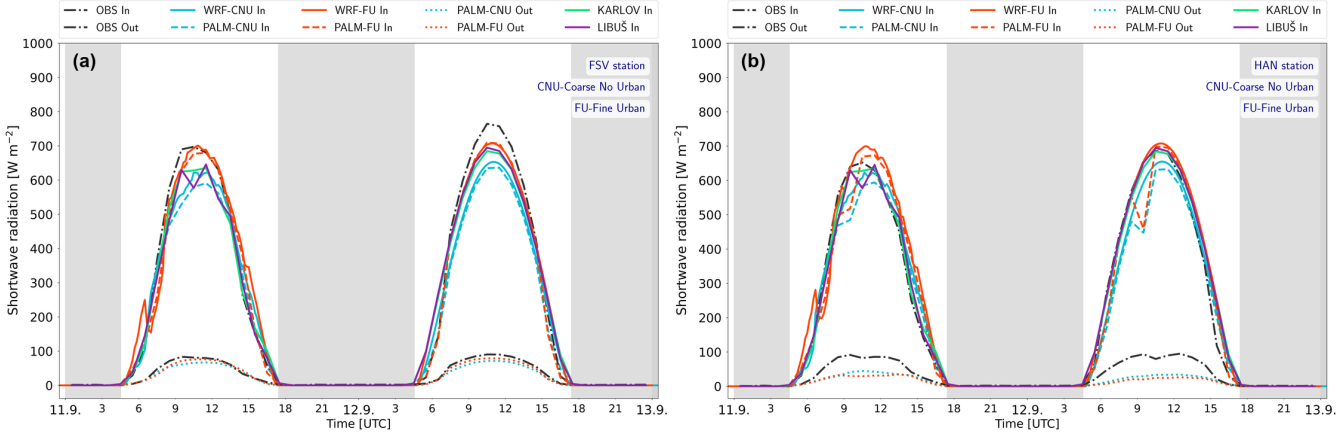

Figure S4. The comparison of observed hourly averages of incoming (In) and outgoing (Out) short-wave radiation for the e6 episode at the stations FSV (a) and HAN (b), with PALM model outputs for both WRF configurations. Additional lines represent the raw WRF outputs, Coarse No Urban (WRF-CNU), and Fine Urban (WRF-FU), and measurements from professional meteorological stations in Karlov and Libuš.

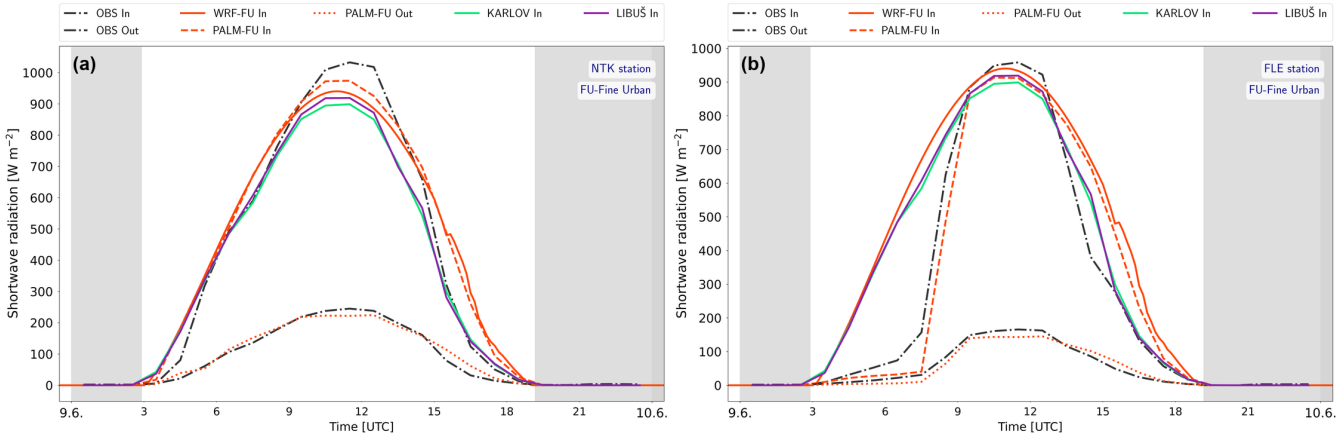

Figure S5. The comparison of observed hourly averages of incoming (In) and outgoing (Out) short-wave radiation for the e7 episode at the stations NTK (a) and FLE (b), with PALM model output for WRF Fine Urban (WRF-FU) configuration. Additional lines represent the raw WRF output, Fine Urban (WRF-FU), and measurements from professional meteorological stations in Karlov and Libuš.

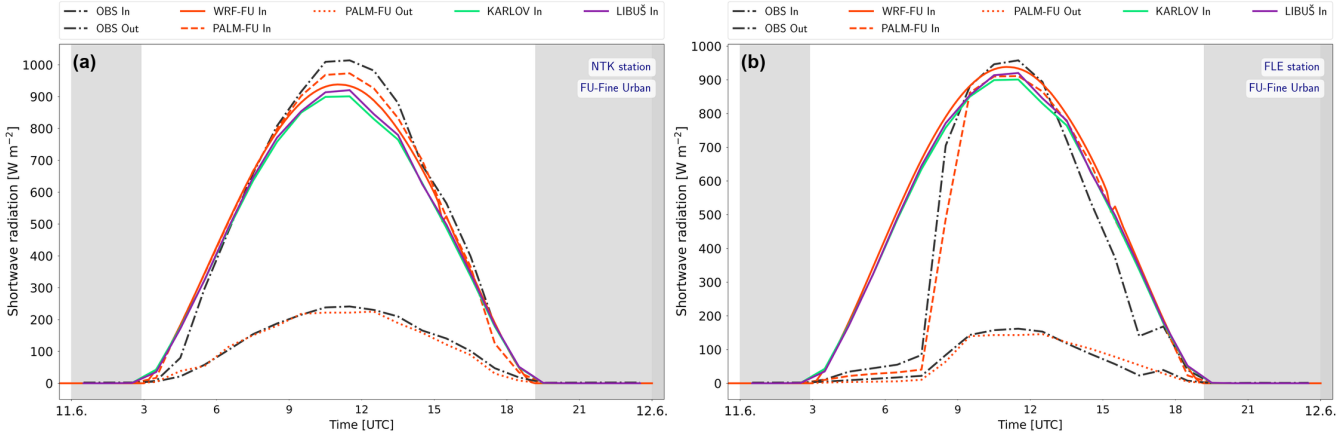

Figure S6. The comparison of observed hourly averages of incoming (In) and outgoing (Out) short-wave radiation for the e8 episode at the stations NTK (a) and FLE (b), with PALM model output for WRF Fine Urban (WRF-FU) configuration. Additional lines represent the raw WRF output, Fine Urban (WRF-FU), and measurements from professional meteorological stations in Karlov and Libuš.

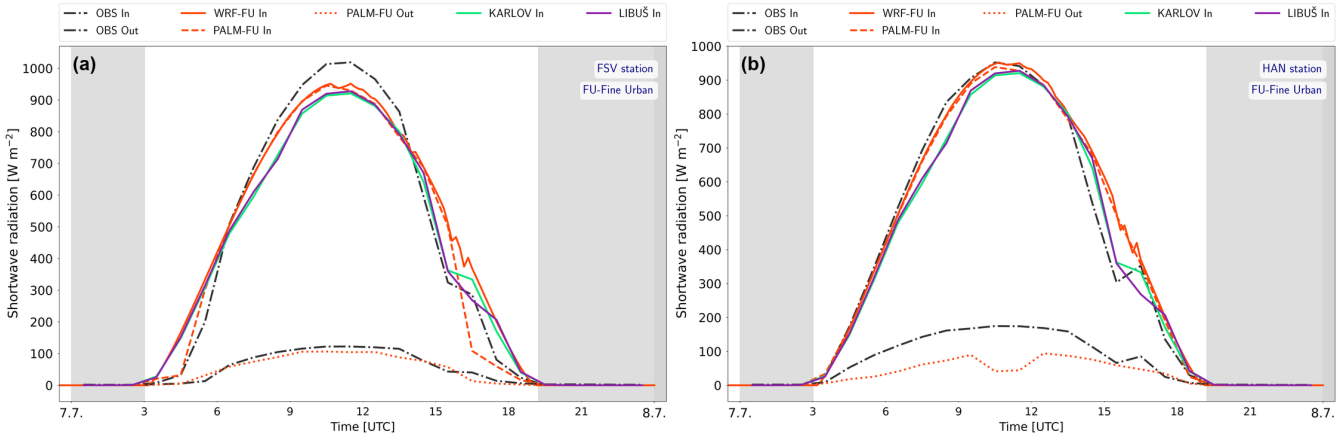

Figure S7. The comparison of observed hourly averages of incoming (In) and outgoing (Out) short-wave radiation for the e11 episode at the stations FSV (a) and HAN (b), with PALM model output for WRF Fine Urban (WRF-FU) configuration. Additional lines represent the raw WRF output, Fine Urban (WRF-FU), and measurements from professional meteorological stations in Karlov and Libuš.

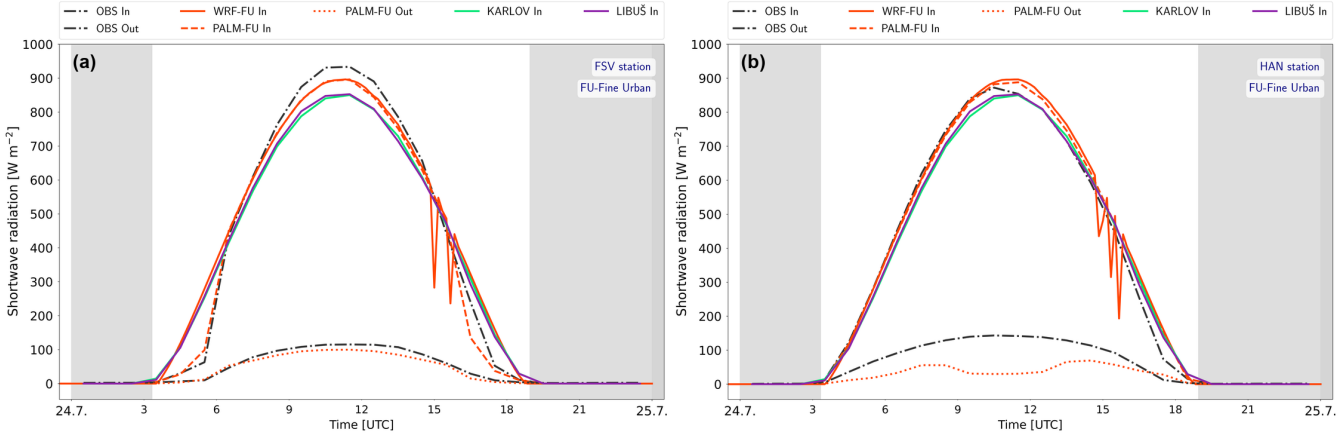

Figure S8. The comparison of observed hourly averages of incoming (In) and outgoing (Out) short-wave radiation for the e13 episode at the stations FSV (a) and HAN (b), with PALM model output for WRF Fine Urban (WRF-FU) configuration. Additional lines represent the raw WRF output, Fine Urban (WRF-FU), and measurements from professional meteorological stations in Karlov and Libuš.

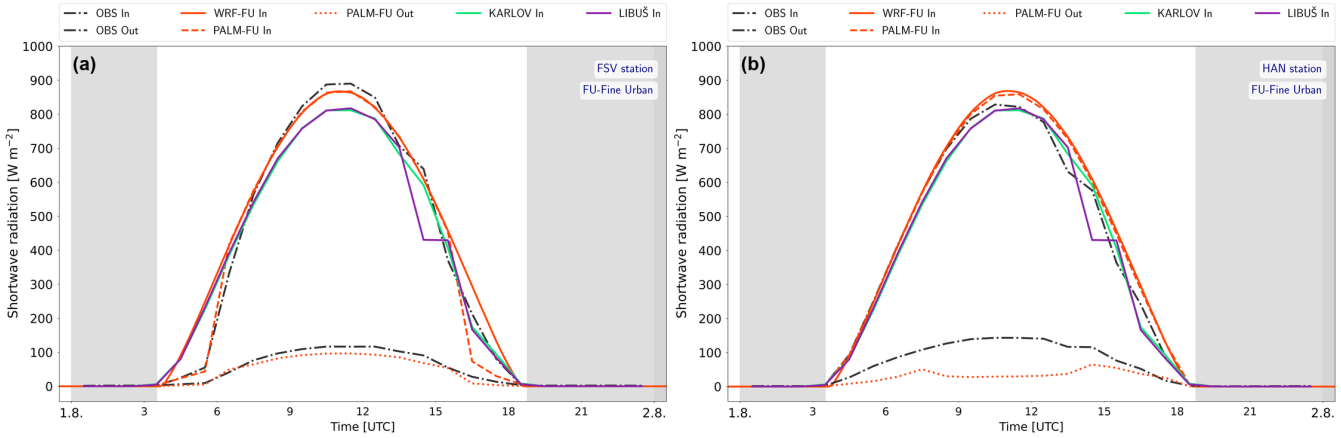

Figure S9. The comparison of observed hourly averages of incoming (In) and outgoing (Out) short-wave radiation for the e14 episode at the stations FSV (a) and HAN (b), with PALM model output for WRF Fine Urban (WRF-FU) configuration. Additional lines represent the raw WRF output, Fine Urban (WRF-FU), and measurements from professional meteorological stations in Karlov and Libuš.

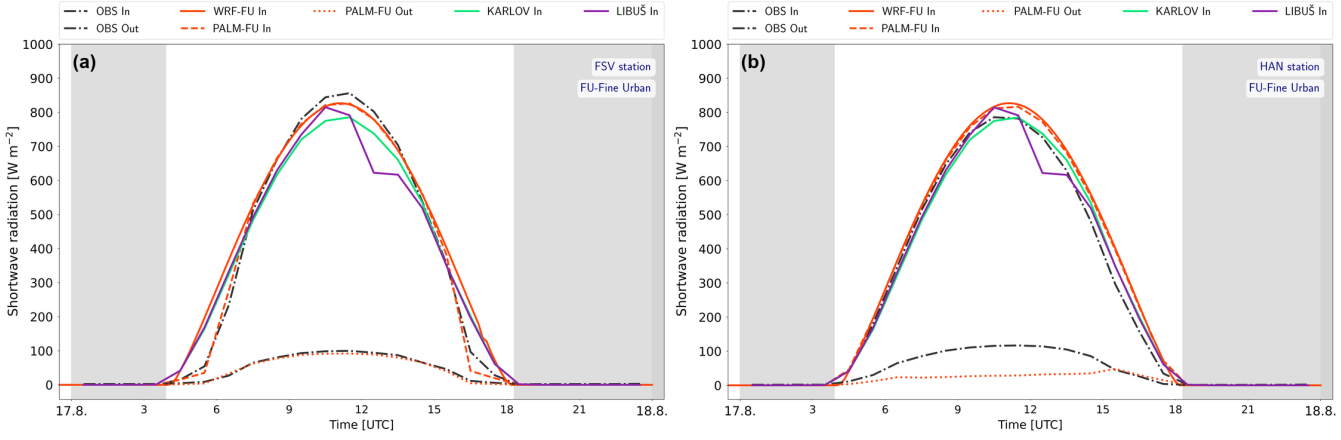

Figure S10. The comparison of observed hourly averages of incoming (In) and outgoing (Out) short-wave radiation for the e15 episode at the stations FSV (a) and HAN (b), with PALM model output for WRF Fine Urban (WRF-FU) configuration. Additional lines represent the raw WRF output, Fine Urban (WRF-FU), and measurements from professional meteorological stations in Karlov and Libuš.

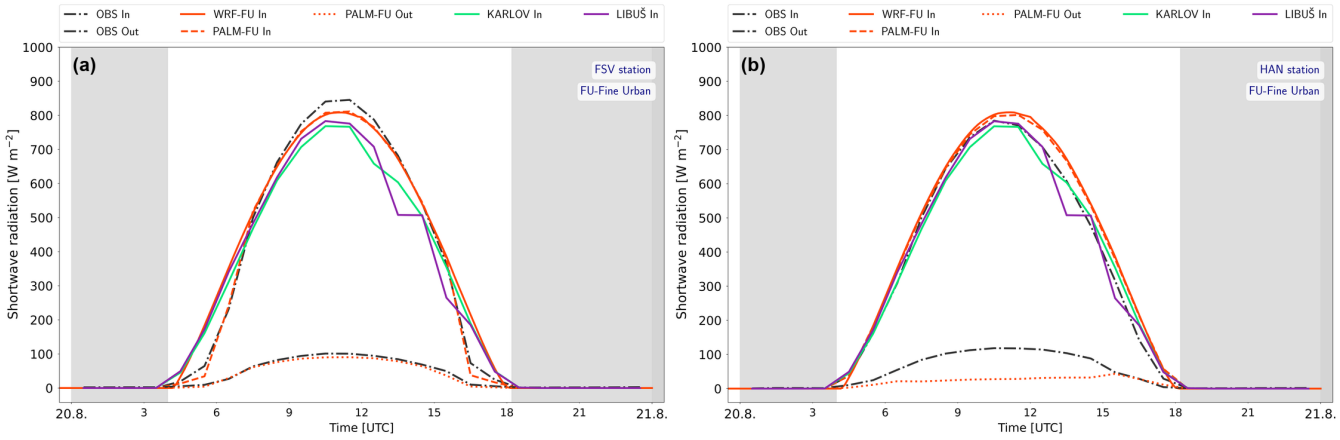

Figure S11. The comparison of observed hourly averages of incoming (In) and outgoing (Out) short-wave radiation for the e16 episode at the stations FSV (a) and HAN (b), with PALM model output for WRF Fine Urban (WRF-FU) configuration. Additional lines represent the raw WRF output, Fine Urban (WRF-FU), and measurements from professional meteorological stations in Karlov and Libuš.

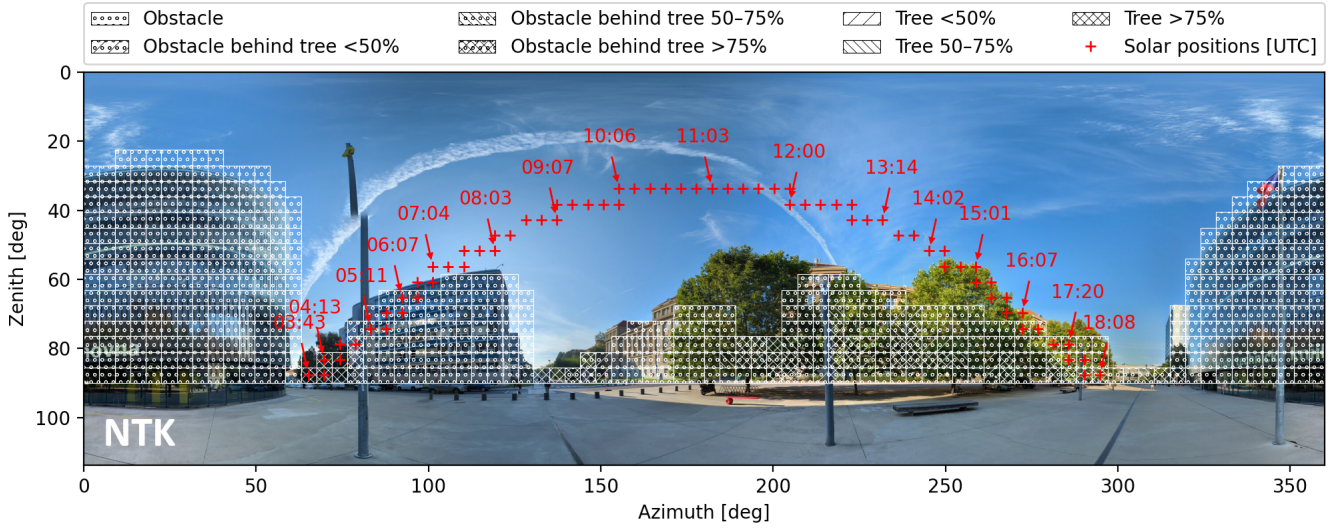

Figure S12. Hemispherical view at the NTK observation site with obstructions and vegetation as modelled by PALM, plotted in azimuth–zenith coordinates. Trees and obstacles are classified according to their fractional area coverage. Red crosses indicate the Sun's trajectory throughout the day, with annotated timestamps in UTC.

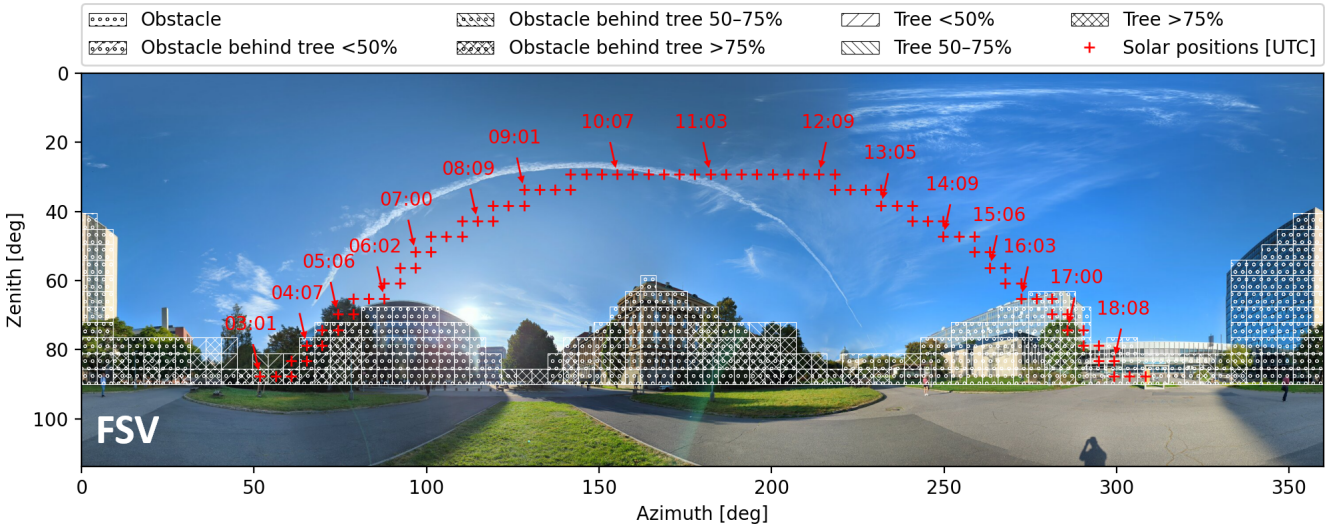

Figure S13. Hemispherical view at the FSV observation site with obstructions and vegetation as modelled by PALM, plotted in azimuth–zenith coordinates. Trees and obstacles are classified according to their fractional area coverage. Red crosses indicate the Sun's trajectory throughout the day, with annotated timestamps in UTC.

Table S1. Synoptic weather types and frontal systems crossing through Prague during selected episodes in 2017 and 2018.

Date	Weather type	Front crossings			
		Crossing time [UTC]	Type	Direction (from)	Intensity
2017					
09 June	Western anticyclone of summer type (Wal)	18	Cold	West	Medium
		23	Cold	West	Medium
11 June	Western anticyclone of summer type (Wal)	7	Warm	South West	Weak
		22	Warm	South West	Weak
19–20 June	Anticyclone/ Travelling anticyclone (A/Ap)	9 (20 Jun.)	Cold	North West	Weak
07 July	Western cyclone (Wc)	1	Cold	Western	Medium
19 July	Western anticyclone of summer type (Wal)	No data	No data	No data	No data
07 August	Traveling anticyclone (Ap)	No data	No data	No data	No data
2018					
16 June	North East anticyclone (Nea)	No data	No data	No data	No data
30 June	North East anticyclone (Nea)	No data	No data	No data	No data
02–03 July	North West anticyclone (NWa)	No data	No data	No data	No data
07 July	North West anticyclone (NWa)	17	Occlusive	North West	Weak
21 July	Low pressure trough (B)	17	Occlusive	South West	Medium
24 July	North West anticyclone (NWa)	No data	No data	No data	No data
01 August	Eastern anticyclone (Ea)	No data	No data	No data	No data
17 August	Western anticyclone of summer type (Wal)	23	Cold	West	Medium
20 August	Western anticyclone of summer type (Wal)	2	Warm	West	Weak
		15	Cold	North West	Medium
11–12 September	Western anticyclone of summer type (Wal)	2 (11 Sept.)	Occlusive	West	Medium
		9 (11 Sept.)	Warm	West	Medium
		12 Sept.	No data	No data	No data

Table S2. WRF albedo during 2017 and 2018 at observation stations. WRF–1 km domain.

Date	Station	Mean Albedo	Albedo at Noon	Albedo (Noon Avg. +-1 h)
2017				
09 June	FLE	0.199	0.156	0.156
	NTK	0.199	0.156	0.156
11 June	FLE	0.173	0.156	0.157
	NTK	0.173	0.156	0.157
19–20 June	FLE	0.174	0.167	0.157
	NTK	0.174	0.167	0.157
07 July	FLE	0.213	0.353	0.228
	NTK	0.213	0.353	0.228
19 July	FLE	0.181	0.157	0.156
	NTK	0.181	0.157	0.156
07 August	FLE	0.180	0.155	0.155
	NTK	0.180	0.155	0.155
2018				
16 June	FSV	0.197	0.156	0.157
	HAN	0.213	0.158	0.158
30 June	FSV	0.172	0.156	0.156
	HAN	0.172	0.158	0.158
02–03 July	FSV	0.173	0.167	0.157
	HAN	0.173	0.167	0.158
07 July	FSV	0.184	0.176	0.192
	HAN	0.183	0.179	0.191
21 July	FSV	0.206	0.169	0.169
	HAN	0.206	0.169	0.169
24 July	FSV	0.184	0.156	0.156
	HAN	0.184	0.158	0.158
01 August	FSV	0.176	0.164	0.163
	HAN	0.176	0.163	0.163
17 August	FSV	0.171	0.154	0.154
	HAN	0.172	0.156	0.156
20 August	FSV	0.170	0.154	0.154
	HAN	0.171	0.156	0.156
11–12 September	FSV	0.190	0.313	0.168
	HAN	0.192	0.309	0.171

Table S3. WRF albedo during 2017 and 2018 at observation stations. WRF–3 km domain.

Date	Station	Mean Albedo	Albedo at Noon	Albedo (Noon Avg. +-1 h)
2017				
19–20 June	FLE	0.144	0.144	0.144
	NTK	0.144	0.144	0.144
19 July	FLE	0.140	0.140	0.140
	NTK	0.140	0.140	0.140
07 August	FLE	0.135	0.135	0.135
	NTK	0.135	0.135	0.135
2018				
30 June	FSV	0.142	0.142	0.142
	HAN	0.152	0.152	0.152
02–03 July	FSV	0.142	0.142	0.142
	HAN	0.151	0.151	0.151
11–12 September	FSV	0.126	0.127	0.126
	HAN	0.132	0.133	0.132

Table S4. Average albedo values per station. WRF–1 km domain.

Station	Avg (Mean)	Avg (Noon)	Avg (Noon Avg)
FLE [213, 149]	0.187	0.190	0.168
NTK [213, 149]	0.187	0.190	0.168
FSV [213, 149]	0.182	0.176	0.162
HAN [213, 148]	0.184	0.177	0.163

Table S5. Average albedo values per station. WRF–3 km domain.

Station	Avg (Mean)	Avg (Noon)	Avg (Noon Avg)
FLE [75, 70]	0.139	0.140	0.139
NTK [75, 70]	0.139	0.140	0.139
FSV [75, 70]	0.137	0.137	0.137
HAN [75, 69]	0.145	0.145	0.145

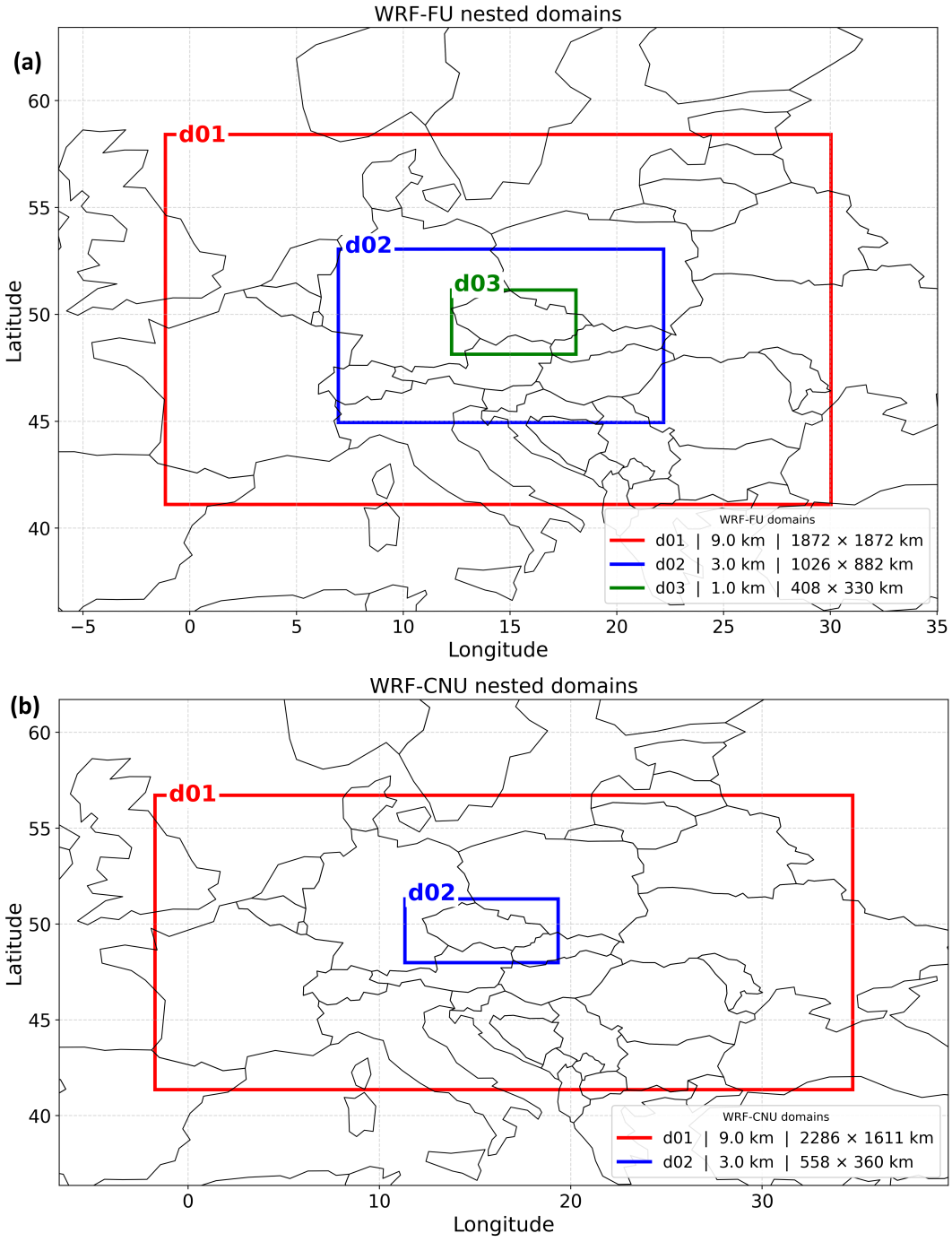

Figure S14. WRF model simulation domain configurations and nested grid hierarchies for the two experimental setups: (a) the three-domain WRF-FU setup (red: d01 at 9.0 km, blue: d02 at 3.0 km, and green: d03 at 1.0 km horizontal resolution) and (b) the two-domain WRF-CNU setup (red: d01 at 9.0 km and blue: d02 at 3.0 km horizontal resolution). The legends denote the horizontal grid spacing and total geographic coverage area for each parent and nested domain.

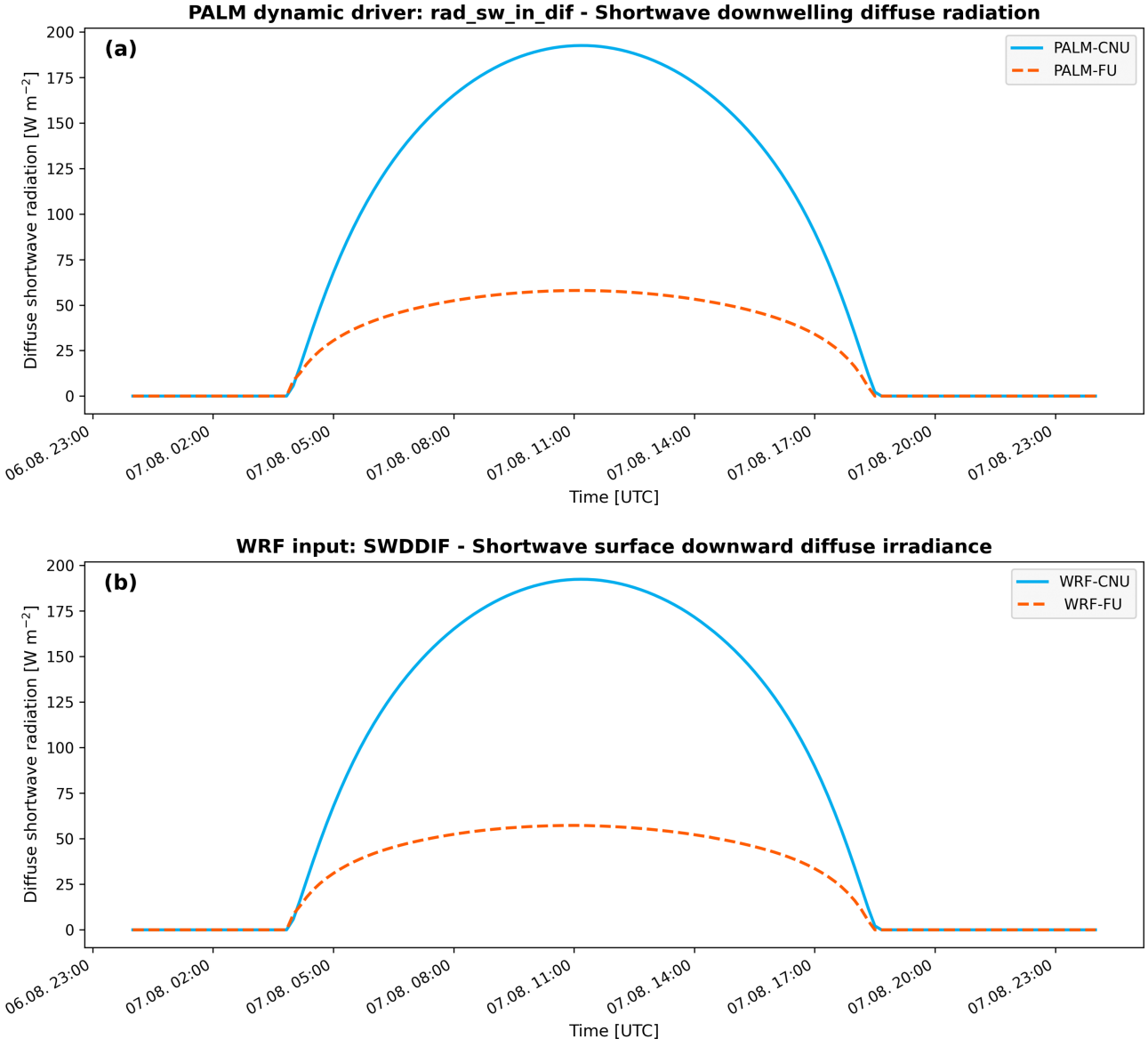

Figure S15. Comparison of diffuse short-wave radiation supplied to PALM-CNU (solid blue) and PALM-FU (dashed orange) setups through the dynamic driver (panel (a); variable rad_sw_in_dif) with the corresponding forcing data from WRF-CNU (solid blue) and WRF-FU (dashed orange) (panel (b); variable SWDDIF) for the clear-sky episode e6 at the FLE station.

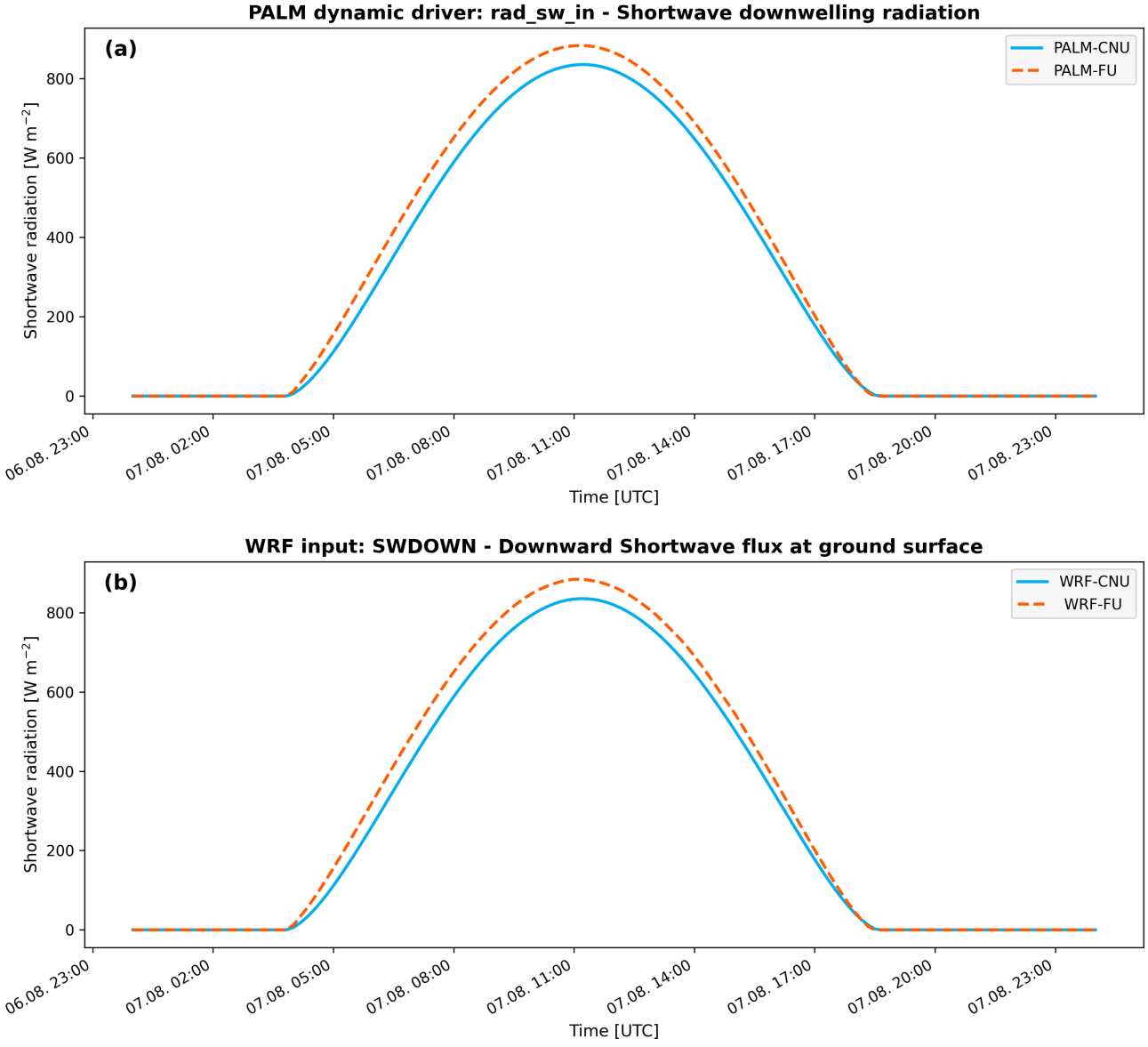

Figure S16. Comparison of the direct short-wave radiation supplied to PALM-CNU (solid blue) and PALM-FU (dashed orange) setups through the dynamic driver (panel (a); variable rad_sw_in) with the corresponding forcing data from WRF-CNU (solid blue) and WRF-FU (dashed orange) (panel (b); variable SWDOWN) for the clear-sky episode e6 at the FLE station.

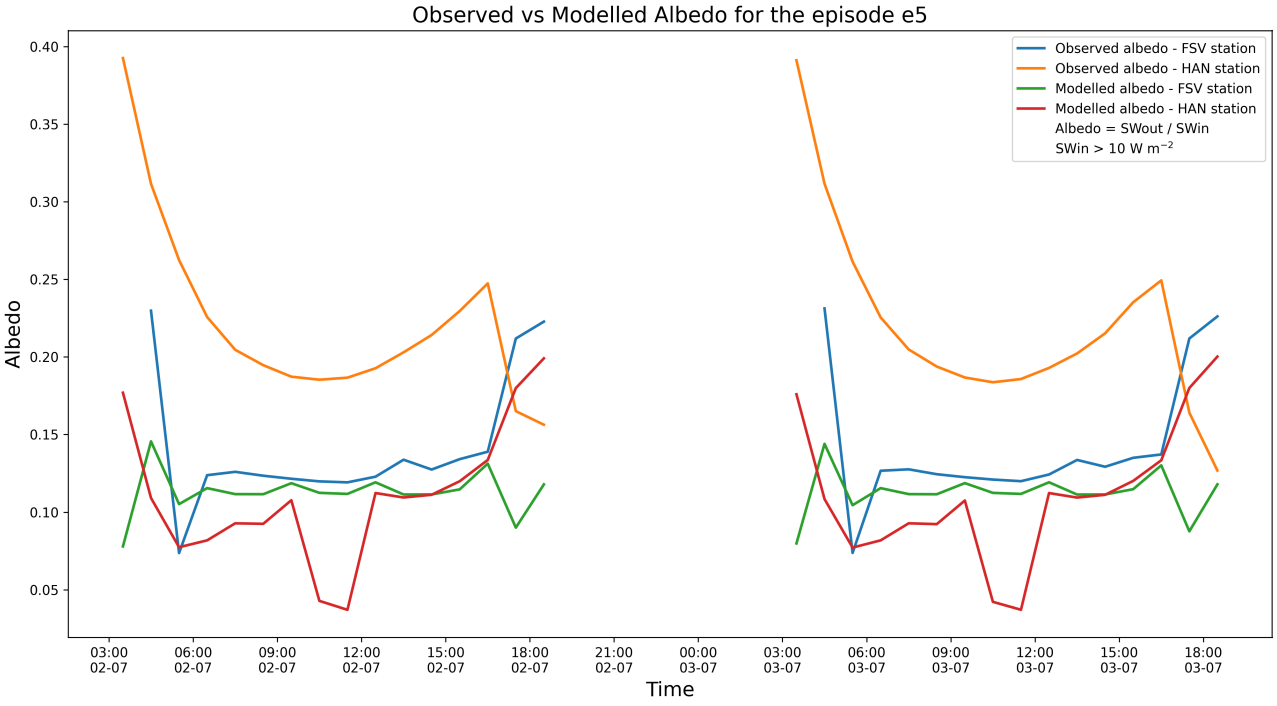

Figure S17. Comparison of observed and PALM-modelled albedo at the FSV and HAN stations during episode e5. Albedo was calculated as the ratio of reflected to incoming short-wave radiation (SWout/SWin). Only periods with incoming short-wave radiation exceeding 10 W m^{-2} were considered.